PLANT SCIENCE

Plant cell wall patterning and expansion mediated by protein-peptide-polysaccharide interaction

Steven Moussu[1]†‡, Hyun Kyung Lee[1]†, Kalina T. Haas[2], Caroline Broyart[1], Ursina Rathgeb[3], Damien De Bellis[3,4], Thomas Levasseur[5], Sébastjen Schoenaers[2,6], Gorka S. Fernandez[7], Ueli Grossniklaus[7], Estelle Bonnin[5], Eric Hosy[8], Kris Vissenberg[6,9], Niko Geldner[3], Bernard Cathala[5], Herman Höfte[2]*, Julia Santiago[1]*

Assembly of cell wall polysaccharides into specific patterns is required for plant growth. A complex of RAPID ALKALINIZATION FACTOR 4 (RALF4) and its cell wall–anchored LEUCINE-RICH REPEAT EXTENSIN 8 (LRX8)–interacting protein is crucial for cell wall integrity during pollen tube growth, but its molecular connection with the cell wall is unknown. Here, we show that LRX8-RALF4 complexes adopt a heterotetrametric configuration in vivo, displaying a dendritic distribution. The LRX8-RALF4 complex specifically interacts with demethylesterified pectins in a charge-dependent manner through RALF4's polycationic surface. The LRX8-RALF4-pectin interaction exerts a condensing effect, patterning the cell wall's polymers into a reticulated network essential for wall integrity and expansion. Our work uncovers a dual structural and signaling role for RALF4 in pollen tube growth and in the assembly of complex extracellular polymers.

A central question in plant biology is how cell wall polymers assemble into specific mesoscale patterns, conferring to the walls their physicochemical properties that allow growth and development. Plant cell walls consist of cellulose microfibrils and matrix polymers, which include the polyanionic pectins. Among the pectins, homogalacturonan is the most abundant polymer in expanding cell walls (*1*). During cell expansion, regulation of homogalacturonan charge through demethylesterification plays a key role in controlling cell wall mechanics (*2*–*5*). Cell expansion needs to be tightly controlled by rapid feedback signaling loops that coordinate cell wall deposition and remodeling to avoid loss of cell wall integrity. Here, we show that RAPID ALKALINIZATION FACTOR 4 (RALF4) peptides are required for cell wall patterning through their interaction with demethylesterified homogalacturonan. RALFs were previously identified as signaling peptides that coordinate the functional integrity of cell walls in a plethora of processes underlying plant development and innate immunity (*6*–*14*). These peptides instruct, in a mutually exclusive way and with different affinities, two structurally distinct protein families, the cell wall–anchored LEUCINE-RICH REPEAT EXTENSIN (LRX) proteins (*9*, *10*, *15*) and a membrane-integral signaling complex composed of LORELEI-like GLYCOLPHOSPHATIDYLINOSITOL (GPI)-ANCHORED PROTEINS (LLGs) and *Catharanthus roseus* RLK1-like receptor kinases (*Cr*RLK1Ls) (*7*, *12*, *14*, *16*). In this study, we used the pollen tube of *Arabidopsis thaliana*, which has a rapidly growing tip, as a model system to investigate the molecular links among RALFs, LRX proteins, and the cell wall matrix during cell expansion.

[1]The Plant Signaling Mechanisms Laboratory, Department of Plant Molecular Biology, University of Lausanne, 1015 Lausanne, Switzerland. [2]Université Paris-Saclay, INRAE, AgroParisTech, Institut Jean-Pierre Bourgin (IJPB), 78000 Versailles, France. [3]Department of Plant Molecular Biology, University of Lausanne, 1015 Lausanne, Switzerland. [4]Electron Microscopy Facility, University of Lausanne, 1015 Lausanne, Switzerland. [5]INRAE, UR1268 BIA, F-44300 Nantes, France. [6]Integrated Molecular Plant Physiology Research (IMPRES), Department of Biology, University of Antwerp, 2020 Antwerp, Belgium. [7]Department of Plant and Microbial Biology & Zurich-Basel Plant Science Center, University of Zurich, 8008 Zurich, Switzerland. [8]IINS, CNRS UMR5297, University of Bordeaux, 33000 Bordeaux, France. [9]Plant Biochemistry & Biotechnology Lab, Department of Agriculture, Hellenic Mediterranean University, Stavromenos PC 71410, Heraklion, Crete, Greece.
*Corresponding author. Email: hermanus.hofte@inrae.fr (H.H.); julia.santiago@unil.ch (J.S.)
†These authors contributed equally to this work.
‡Present address: Laboratoire de Recherche en Sciences Végétales, Université de Toulouse, CNRS, UPS, Toulouse INP, 31320 Auzeville Tolosane, France.

LRX-bound RALF4 interacts with charged homogalacturonan

Our previous structural analysis of the LRX8-RALF4 signaling complex in the pollen tube revealed that RALF4 peptides, when bound to LRX8, expose an alkaline surface patch rich in Lys and Arg residues (*10*) (Fig. 1A). We hypothesized that this surface patch could serve as a platform to interact with negatively charged cell wall polysaccharides such as pectins. The pollen tube grows inside the pistil toward the ovule and must navigate through various tissues, counterbalancing different physical forces (*17*, *18*). Along this journey, the cell wall at the pollen tube apex constantly needs to adjust its mechanical properties to allow rapid growth while avoiding its rupture (*2*, *3*, *19*). Pectin charge plays a key role in this process (*3*–*5*).

We initially compared the melting profile of recombinantly expressed LRX8 and LRX8-RALF4 complexes (*10*) in the presence and absence of fully demethylesterified homogalacturonan fragments (6- to 15-mer oligogalacturonans hereafter referred as OGs) in thermal shift assays (TSAs) (*20*) (Fig. 1, B and C, and fig. S1). Consistent with our isothermal titration calorimetry (ITC) experiments, these assays revealed an increase in melting temperature (T_m) of LRX8 upon binding to RALF4 (Fig. 1, B and C) (*10*). The T_m further increased in the presence of OGs, whereas no such changes were observed for LRX8 alone (Fig. 1, B and C, and fig. S1). In addition, the LRX8-RALF4 complex did not bind shorter homogalacturonan fragments (fig. S1), a structurally divergent acidic polysaccharide (polymannuronic acid), a negatively charged polymer (DNA), or an unrelated carbohydrate (sucrose) (Fig. 1D and fig. S1). We next quantified these interactions by titrating OGs into an LRX8-RALF4 solution (*10*) using ITC (*21*). LRX8-RALF4 bound OGs at ~2 μM affinity and a binding stoichiometry (N) of 2, suggesting that one OG molecule binds to each of the two RALF4 molecules in the heterotetrametric (2 + 2) LRX8-RALF4 complex (*10*) (Fig. 1E and fig. S2). Consistently, a monomeric version of the complex, monomeric LRX8-RALF4 (*10*), bound one OG molecule (N = 1) with comparable affinity (~2.9 μM), and its T_m increased in the presence of OGs (Fig. 1E and fig. S2). LRX2, a protein that is not expressed in pollen tubes, in complex with RALF4, bound OGs with a similar dissociation constant (1.6 μM) and stoichiometry (Fig. 1E and fig. S2). No binding was detected when titrating OGs into a solution containing either LRX8 alone or free RALF4 or when titrating DNA into the LRX8-RALF4 complex (Fig. 1E and fig. S2). These experiments demonstrate that the LRX-RALF4 complex can bind homogalacturonan oligomers with high affinity and specificity.

During pollen tube growth, demethylesterification at the apex changes the overall electrostatic charge of homogalacturonan, which plays a role in controlling cell wall expansion (*3*, *5*, *22*). The degree of methylation (DM) of homogalacturonan was critical for the interaction with LRX8-RALF4, as shown by its increased thermostability in the presence of non- or low-methylesterified (DM5 = 5% methylesterified) OGs (increase in T_m of 3.9° and 2.5°, respectively), but not of highly methylesterified ones (DM71) (Fig. 1F and fig. S2). Similar results were obtained when using longer pectin chains: The shift in T_m for DM20 pectin occurred at lower concentrations compared with DM43 pectins (Fig. 1G and fig. S2). These results show that LRX8-RALF4 specifically interacts with demethylesterified pectins.

To understand the interaction between LRX8-RALF4 and demethylesterified pectins in molecular terms, we mapped and probed the basic surface of the LRX8-bound RALF4 peptide (*10*) (Fig. 1A). We mutated residues

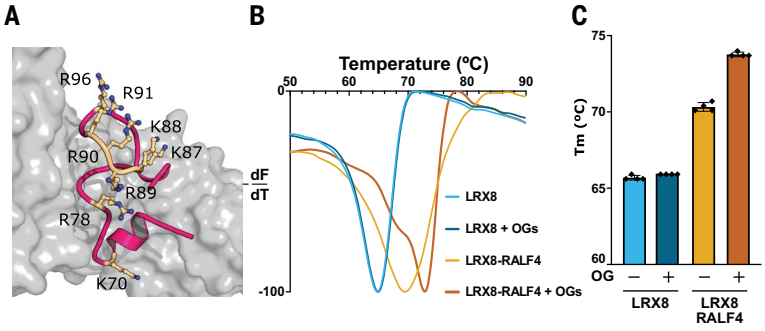

D

		Mock	OGs	Mannuronic Acid	DNA	Sucrose
LRX8	Tm	65.7	65.9	66.2	66.0	66.0
	ΔTm		0.2	0.5	0.3	0.3
LRX8-RALF4	Tm	70.3	73.8	71.2	69.7	69.8
	ΔTm		3.4	0.9	-0.7	-0.5

E

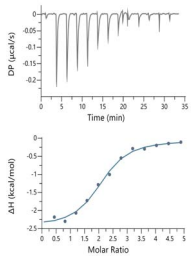

Ligand (syringe)	Protein (cell)	Kd (µM)	ΔH (kcal/mol)	N
OGs	LRX8-RALF4	2 ± 0.5	-2.5 ± 0.1	2
OGs	mLRX8-RALF4	2.9 ± 0.4	-1.8 ± 0.6	1
OGs	LRX8	n.d		
OGs	RALF4	n.d		
OGs	LRX2-RALF4	1.6 ± 0.2	-1.4 ± 0.11	2
DNA	LRX8-RALF4	n.d		

F

		Mock	OG	OG-DM5	OG-DM71
LRX8-RALF4	Tm	68.8	72.7	71.3	69.1
	ΔTm		3.9	2.5	0.3

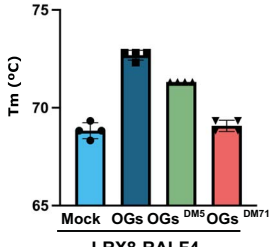

G

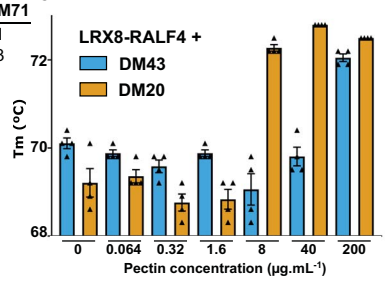

H

Ligand		Pectin concentration (µg/mL) 0	0.064	0.32	1.6	8	40	200
DM43	Tm	69.2	69.9	69.6	69.9	69.1	69.8	72.0
	ΔTm		0.7	0.4	0.7	-0.1	0.6	2.8
DM20	Tm	70.1	69.4	68.8	68.8	72.3	72.8	72.5
	ΔTm		-0.7	-1.3	-1.3	2.2	2.7	2.4

I

		LRX8-RALF4$_{R89E.R90E.R91E}$	LRX8-RALF4$_{neutral\ surface}$
Mock	Tm	73.7	73.4
+ OGs	Tm	74.6	72.1
	ΔTm	**0.9**	**-1.3**

Ligand (syringe)	Protein (cell)	Kd (µM)	ΔH (kcal/mol)	N
OGs	LRX8-RALF4$_{R89E.R90E.R91E}$	8.5 ± 0.4	-5.6 ± 1.6	2
OGs	LRX8-RALF4$_{neutral\ surface}$	n.d.		

J

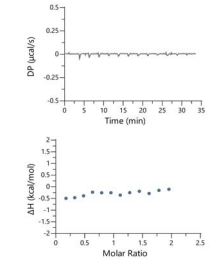

Fig. 1. LRX-bound RALF4 specifically interacts with demethylesterified homogalacturonan in a charge-dependent manner. (**A**) Structural representation of the polycationic interface of RALF4 when bound to LRX8 [Protein Data Bank identifier: 6QWN (*10*)]. LRX8 is depicted in surface representation (gray) and RALF4 as a pink ribbon diagram. Positively charged amino acids in the exposed RALF4 interface are depicted as yellow sticks. (**B**) LRX8-bound RALF4 binds demethylesterified homogalacturonan. Representative thermal denaturation profiles of LRX8 and LRX8-RALF4 in the absence and presence of OGs. (**C**) Graphical representation of T_m of different TSAs shown in (B). Data are shown as means ± SD of four independent experiments. (**D**) Summary table of T_m and ΔT_m of LRX8 and LRX8-RALF4 in the presence of OGs and control molecules (n = 4). (**E**) ITC thermogram of LRX8-RALF4 versus OGs (left) and ITC summary table (right) of LRX8 alone, RALF4, and LRXs-RALF4 versus OGs and DNA oligomers. K_d (dissociation constant) indicates the binding affinity between the two molecules considered (in micromolar). N is the reaction stoichiometry (N = 1 for a 1:1 interaction). The values indicated in the table are shown as means ± SD of at least two independent experiments. n.d., no detectable binding. (**F**) Summary table (top) and representation of T_m (bottom) of LRX8-RALF4 versus OGs and OGs with different degrees of methylesterification (e.g., DM71 = 71% methylesterification). Data are shown as means ± SD; n = 4. (**G**) T_m bar representation of LRX8-RALF4 in the presence of increasing concentrations of long chains of homogalacturonan with DM43 and DM20. Data are shown as means ± SD; n = 4. (**H**) Summary table of the T_ms shown in (G). (**I** and **J**) Mutation of RALF4 polycationic surface disrupts the interaction with homogalacturonan. (I) Summary table of T_ms of RALF4$_{R89E.R90E.R91E}$ and RALF4$_{neutral\ surface}$ variants in the presence of OGs. (J) ITC of RALF4$_{neutral\ surface}$ versus OGs (left). (Right) ITC summary table of RALF4$_{R89E.R90E.R91E}$ and RALF4$_{neutral\ surface}$ mutants versus OGs. The values indicated in the table are shown as the means ± SD of at least two independent experiments.

in RALF4's basic patch to either Ala or Glu, and recombinantly expressed two mutant variants of the LRX8-RALF4 complex, one targeting the protruding loop of the folded signaling peptide (RALF4$_{R89E.R90E.R91E}$) and the other neutralizing the basic surface altogether (RALF4$_{K70A.R78A.K87A.K88A.R89A.R90A.R91A.R96A}$; hereafter referred as RALF4$_{neutral\ surface}$) (Fig. 1A and fig. S3). Both RALF4 mutants still bound LRX8 and LLG3 with wild-type–like affinity (fig. S3) (*10*). However, TSAs failed to detect an OG-induced increase in T_m for both LRX8-bound RALF4 mutants (Fig. 1, B to D and I, and fig. S4). Consistent with these findings, LRX8-RALF4$_{neutral\ surface}$ and LRX8-RALF4$_{R89E.R90E.R91E}$ showed either no or about a fourfold reduced OG-binding relative to the wild-type complex in ITC assays, respectively (Fig. 1, E and J, and fig. S4). Together, these results confirm the electrostatic nature of the interaction between LRX8-RALF4 and pectin.

LRX8, RALF4, and pectin form a reticulated pattern in vivo

Next, we investigated whether LRX8, RALF4, and pectin also interact in vivo. To this end, we performed immunolabeling and high-resolution

microscopy on pollen tubes expressing functionally tagged RALF4-HA and LRX8-myc under their native promoters (fig. S5) (*10*). Consistent with our structural and biochemical data (*10*), both proteins colocalized in pollen tube cell walls, suggesting that the complex is also present in vivo. However, the complex was present all along the pollen tube cell wall (Fig. 2A and fig. S6), not just at the tip, where the peptide and LRX8 are secreted. This indicates that RALF4, like LRX8, become an integral part of the pollen tube cell wall, which is an unexpected finding for a signaling peptide. This was confirmed by dSTORM super-resolution microscopy (*23*, *24*), which revealed a comparable distribution for the RALF4-HA peptide and LRX8-myc in punctate domains forming a reticulated network (Fig. 2, B and D). Moreover, cluster-size analysis of LRX8-myc and RALF4-HA was consistent with the presence of either one or two copies of the tags in each puncta, indicating the presence of heterotetrametric complexes in vivo (Fig. 2, C and E) (*10*). Concerning the distribution of demethylesterified homogalacturonan, Airyscan and dSTORM microscopy showed that the LM19 immunolabel for demethylesterified pectin

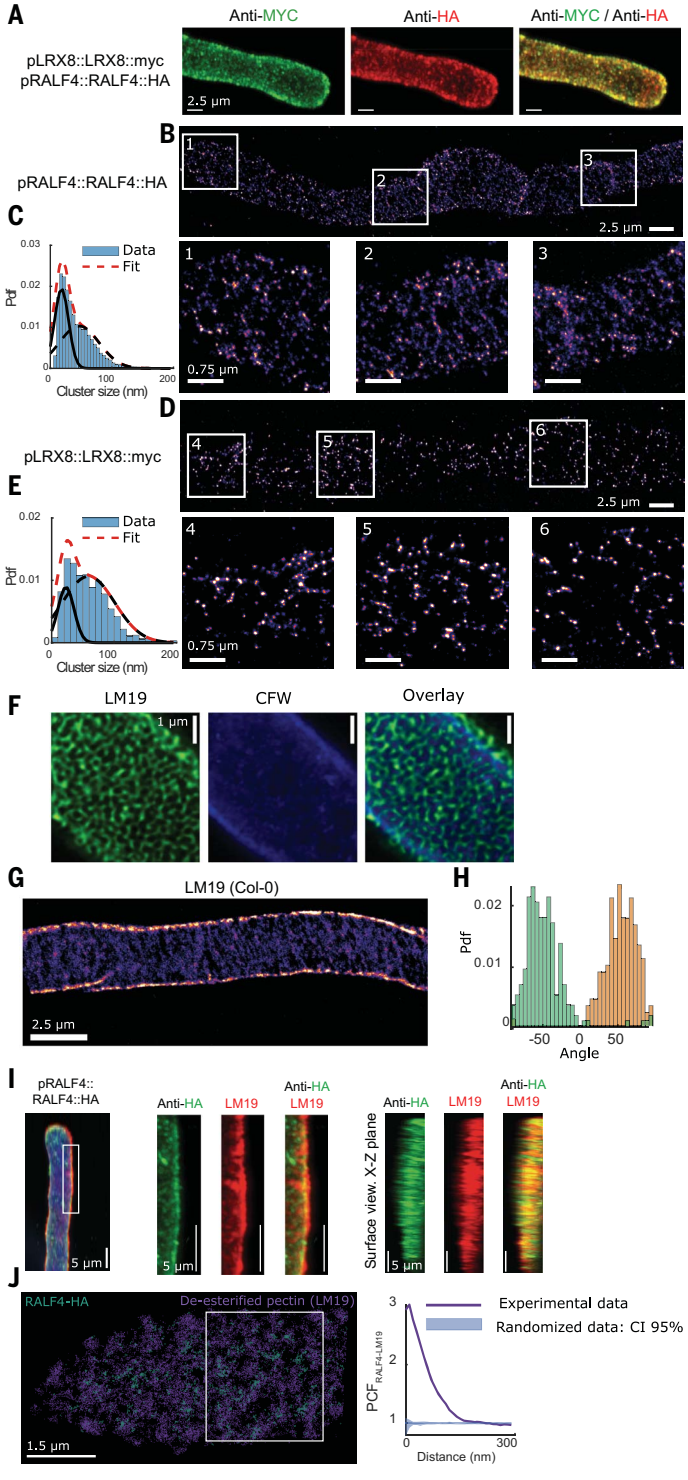

Fig. 2. LRX8, RALF4, and pectin associate in vivo and form a reticulated pattern. (**A**) Representative immunolabeled pollen tube images of a transgenic line expressing LRX8-myc and RALF4-HA under their native promoter in the Col-0 accession. (**B**) Representative pollen tube dSTORM image of immunolabeled *pRALF4::RALF4::HA* in Col-0. Bottom: Magnification of the corresponding squared regions marked in the pollen tube shank shown above. (**C**) Histogram of RALF4-HA probability density function (Pdf) versus cluster size (blue). Fit of the Gaussian mixture model shows two cluster populations with a mean size of 18 nm (monomer 35%) and 47 nm (dimers 65%). A total of 1137 clusters were analyzed from seven pollen tubes from four plants. (**D**) Top: Representative pollen tube dSTORM image of immunolabeled *pLRX8::LRX8::myc* in Col-0 background. Bottom: Magnification of the corresponding squared regions marked in the pollen tube shank shown above. (**E**) Histogram of LRX8-myc Pdf versus cluster size (blue). Two cluster populations of Gaussian mixture shows mean sizes of 23 nm (monomers 46%) and 59 nm (dimers 54%). A total of 937 clusters were analyzed from seven pollen tubes from four plants. (**F**) Representative orthogonal projection of Airyscan *z* stacks of demethylesterified homogalacturonan labeled with LM19 in wild-type pollen tubes. Calcofluor white (CFW) signal, mainly staining callose, did not show a patterned distribution. (**G**) Representative dSTORM image of a wild-type pollen tube labeled with LM19. (**H**) Histogram of Pdf versus angle, showing two distinct populations of pectin filaments (n = 4). (**I**) Confocal images of sequential immunolabeling targeting *pRALF4::RALF4::HA* in Col-0, and LM19 in pollen tube shanks. Maximal intensity *Z*-projected image (middle) and pollen tube surface view of the *X*–*Z* plane (right). (**J**) Left: Representative pollen tube dSTORM image with immunolabeled *pRALF4:RALF4-HA* and LM19. Right: Bivariate point correlation function (PCF) analysis calculated between RALF4-HA (green) and LM19 (violet) compared with the PCF calculated on randomized datasets. The PCF of experimental data lies above the 95% randomization confidence interval (CI), indicating spatial association between the protein and the polysaccharide.

(*25*) was not distributed randomly, as would be expected for an amorphous pectin gel, but rather formed an interconnected pattern of fibers (Fig. 2, F and G, and figs. S7 and S8) (*26*, *27*). This observed architecture is reminiscent of previously described ring like pectin bands in pollen tubes (*28*, *29*). The pattern presented a bimodal angle distribution, displaying as LRX8-RALF4, a web-like network (Fig. 2, F to H, and figs. S7 and S8). The interaction of LRX8-RALF4 with demethylesterified homogalacturonan in vivo was corroborated by the colocalization of RALF4-HA with LM19 antibodies in a periodic banding pattern at the pollen tube surface (Fig. 2I). This was confirmed at higher resolution by dSTORM microscopy, in which a two-point correlation function analysis showed that domains containing LM19-labeled pectin and RALF4-HA were not distributed independently of each other, but rather were associated in space, exhibiting a reticulated pattern (Fig. 2J and fig. S9).

Cell wall patterning and integrity through LRX8-RALF4-pectin compaction

The reticulated pattern of the LM19-labeled pectin and RALF4-HA domains could indicate the association of LRX8-RALF4 with preexisting fibrous structures or a more active role of the complex in the patterning of the cell wall polysaccharides. To investigate the latter possibility, we first studied in vitro how exposure to LRX8-RALF4 affects the rheology of a pectin layer using quartz-crystal microbalance with dissipation monitoring (QCM-D) (*21*, *30*). Briefly, to prepare the pectin layer, a pectin solution (DM43) was poured over an oscillating quartz crystal coated with a polycationic polymer while monitoring the frequency (ΔF, negative for a mass increase) and dissipation rate of the oscillation upon interruption of the current (ΔD, positive for increase in viscoelasticity of the layer). The drop in ΔF and increase in ΔD indicated the formation of an elastic pectin layer (Fig. 3A and fig. S10). The addition of free RALF4 induced an increase in ΔF rather than a decrease, which would be expected for the binding of the peptide, and a strong decrease in ΔD. This is consistent with an electrostatic interaction between the cationic RALF4 and anionic pectin, causing the hydrated pectin layer to dewater and stiffen. The increase in ΔF indicates that the mass loss due to dewatering exceeds the mass gain due to the binding of the small 5.6-kDa peptide. The RALF4-pectin interaction was reversible, as shown by the slow reversal of ΔF and ΔD during a subsequent washing step (Fig. 3B and fig. S10). Addition of LRX8-RALF4 to the pectin layer resulted in an amplified decrease in ΔF and ΔD (Fig. 3B). Here, the mass increase of the much larger complex (110 kDa) exceeded the mass of the expulsed water, explaining the decrease in ΔF. The complex, in contrast to the free RALF4 peptide, had a lasting condensing effect on the pectin layer, because ΔF and ΔD did not reverse during the washing step (Fig. 3B). Consistent with our previous binding assays, LRX8 alone did not induce any changes either in frequency (binding) or pectin rigidification, confirming that RALF4 targets the complex to pectins. The

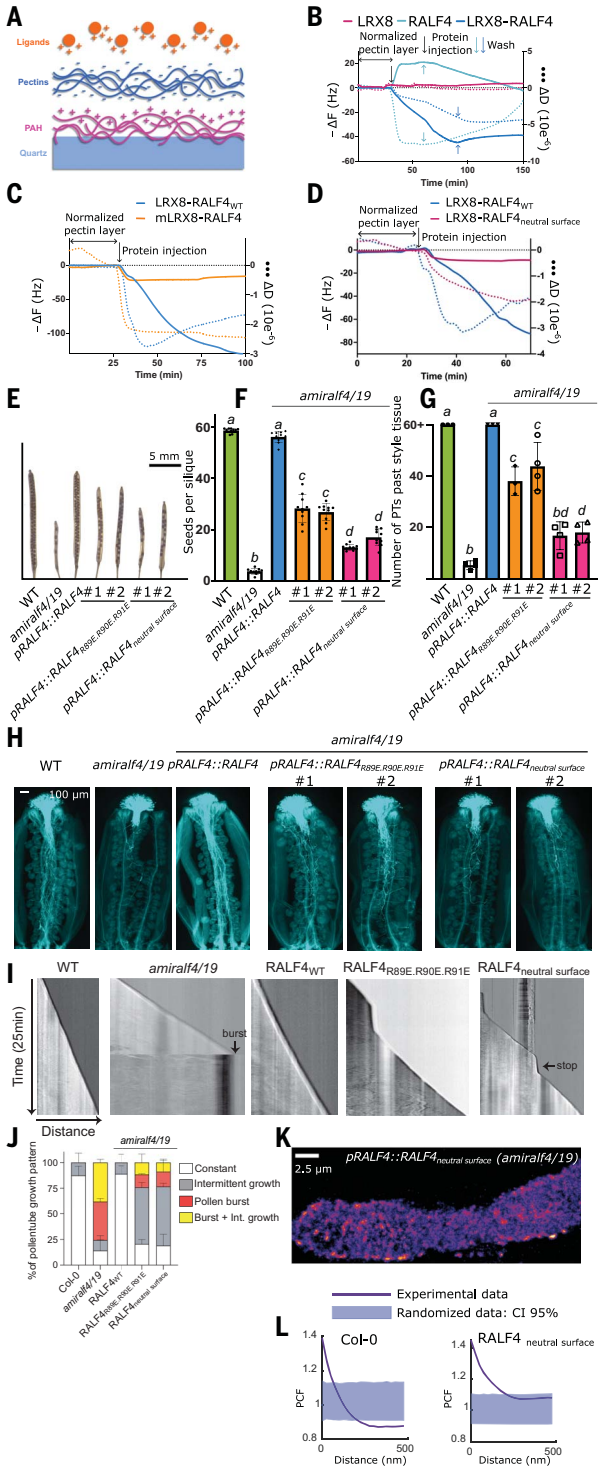

Fig. 3. LRX8-RALF4–induced pectin compaction promotes cell wall patterning regulating pollen tube growth. (**A**) Schematic overview of the QCM-D binding experiments (fig. S10). (**B** to **D**) Representative QCM-D profiles corresponding to the frequency (ΔF, solid lines), and dissipation (ΔD, dotted lines). Protein was injected over a DM43 pectin layer during the period indicated by the arrowheads. (B) QCM-D representative profiles of injecting RALF4 (light blue) (n = 7), LRX8-RALF4 (dark blue) (n = 16), and LRX8 (pink) (n = 3). (C) Representative profiles of dimeric LRX8-RALF4 (blue) (n = 16) and monomeric LRX8-RALF4 (orange) (n = 3). (D) Representative profiles of LRX8-RALF4 (blue) (n = 16), and LRX8-RALF4 $_{\text{neutral surface}}$ (pink) (n = 4). (**E** and **F**) Seeds per silique of Col-0 (wild-type, WT), *amiralf4/19*, *pRALF4::RALF4*$_{WT}$, and RALF4 mutants. Error bars are ± SD; n = 3. (**G**) Number of survived pollen tubes past style tissue. Error bars are ± SD; n = ~3 to 4. $P < 0.0001$, one-way ANOVA with Tukey's multiple-comparisons HSD test. (**H**) Representative images of pollinated *Arabidopsis* pistils stained with aniline blue. Pollen from Col-0, *amiralf4/19*, *pRALF4::RALF4*$_{WT}$, and RALF4 mutants was applied to Col-0 stigmas. (**I**) Representative images of growth kymographs. Arrows indicate either pollen tube bursting or stopping. (**J**) Quantification of growth patterns from kymographs shown in (I). Error bars are ± SD, 15 pollen tubes each; n = 2. (**K**) Representative dSTORM image of LM19 on pollen tubes from *amiralf4/19* complemented with *pRALF4::RALF4*$_{\text{neutral surface}}$. Data are represented as a two-dimensional pixelated image (pixel size, 15 nm). (**L**) Univariate PCF analysis calculated on LM19 dSTORM pointillist data on pollen tubes from Col-0 (left, representative image in Fig. 2G) and *amiralf4/19* complemented with *pRALF4::RALF4*$_{\text{neutral surface}}$ (right). PCF analysis of the distribution of the LM19 epitope shows that the signal crosses the CI in wild-type PTs at shorter distances relative to *pRALF4::RALF4*$_{\text{neutral surface}}$. This indicates that the LM19 epitope in wild-type pollen tubes forms densely packed, spatially segregated fibers compared with the *RALF4*$_{\text{neutral surface}}$ variant.

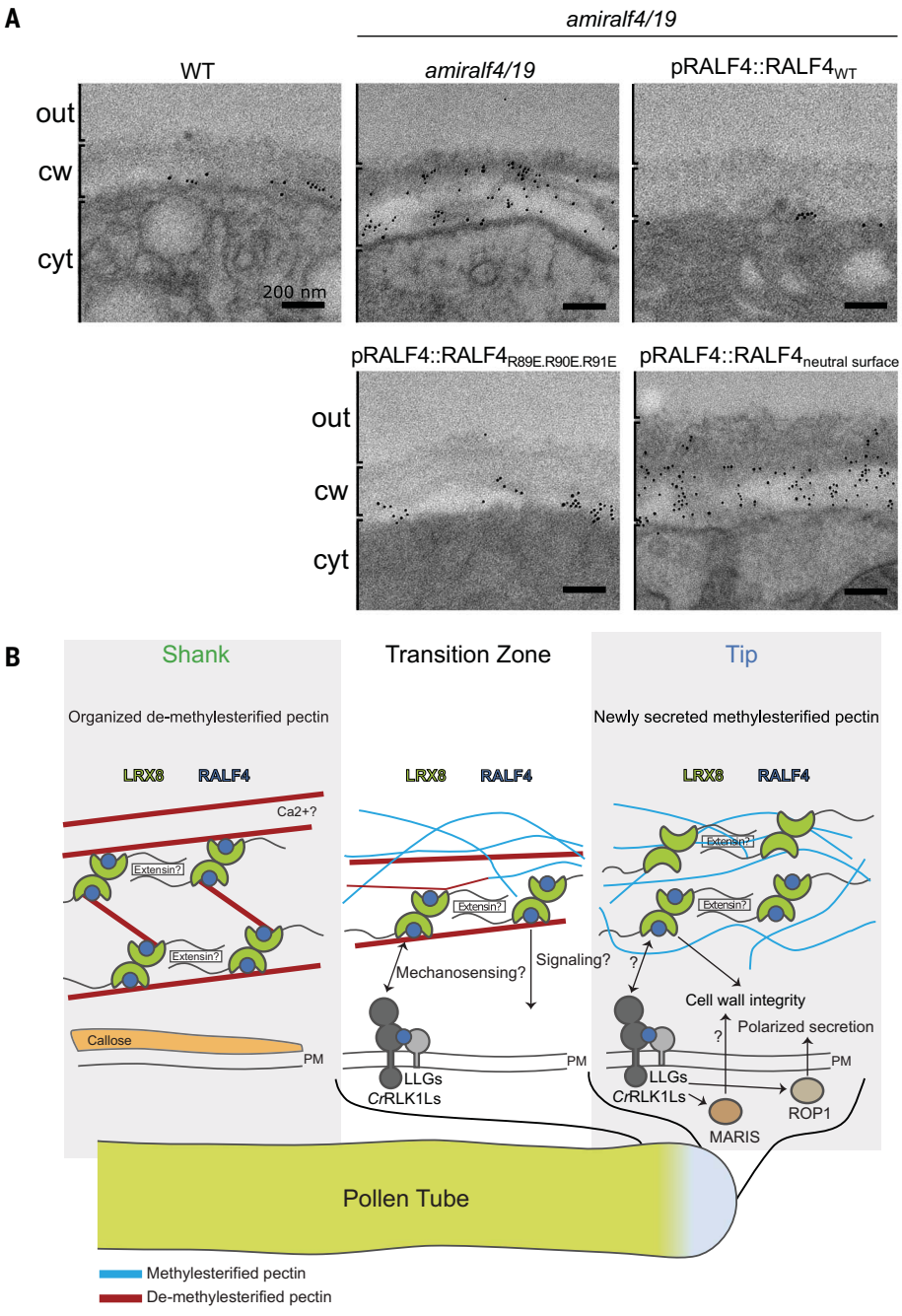

Fig. 4. LRX-RALF4-pectin patterning is required for cell wall assembly and integrity. (**A**) RALF4 surface variants display an aberrant cell wall architecture. Shown are TEM micrographs of pollen tube transverse sections (~10 μm) of Col-0 (WT), *amiralf4/19*, and complementation lines expressing *pRALF4::RALF4*$_{WT}$ *pRALF4::RALF4*$_{R89E.R90E.R91E}$, and *pRALF4::RALF4*$_{neutral\ surface}$. Black dots indicate immunogold labeling for callose. Out, outside; cw, cell wall; cyt, cytoplasm. (**B**) Proposed molecular model of the two RALF4-activated interacting protein families that maintain pollen tube cell wall integrity during growth. Methyl-esterified and de-methyl-esterified pectin are depicted as blue and red lines, respectively. At the tip, membrane-spanning *Cr*RLK1Ls and LLGs sense RALF4/19 to activate downstream MARIS and ROP1 proteins to regulate actin dynamics and promote the polarized secretion of cell wall components and regulatory proteins. At the transition zone, pectin shifts to the demethylesterified form through pectin methylesterase activity (*3*) and is then recognized by the LRX-RALF4 complex. The reticulated network of LRX-RALF4 compacts and chaperones the demethylesterified pectin into a criss-crossed filament network. This network contributes to the patterning, reinforcement, and expansion of the cell wall. At the shank, pectin de-methylesterifcation is complete, and the LRX-RALF4-pectin complex remains an integral part of the pollen cell wall. We speculate that the LRX-RALF4-pectin network acts as a load-bearing system during pollen tube expansion, compensating for its low cellulose content. The modularity of the LRX-extensin network, through the binding of different RALF peptides, would allow targeting and connecting different cell wall polymers or epitopes during cell wall assembly. How the RALF4 membrane and cell wall systems communicate, how these architectural changes in the cell wall are sensed by the pollen tube cell, and whether the peptide can navigate between the two systems will be interesting topics of future studies.

monomerized LRX8-RALF4 complex also induced pectin stiffening (negative ΔD) but showed a greatly reduced pectin-binding capacity (ΔF) relative to the dimeric protein (Fig. 3C), suggesting functional differences depending on the oligomeric state of the complex. The charge dependence of the pectin interaction was confirmed by the strongly reduced pectin binding and condensing capacity of LRX8-RALF4$_{neutral\ surface}$ (Fig. 3D).

These results demonstrate that LRX8-RALF4 has the capacity to recognize and condense demethylesterified pectins in a charge-dependent way. To investigate whether this capacity may direct the patterning of the pollen tube cell wall and affect cell expansion, we generated complementation lines of the *amiralf4/19* line (*9*) by expressing artificial microRNA (amiRNA)–resistant versions of RALF4$_{WT}$, RALF4$_{R89E.R90E.R91E}$, and RALF4$_{neutral\ surface}$ under the control of the native RALF4 promoter (fig. S11). The two RALF4 variants colocalized with LRX8 in the cell wall (figs. S5 and S12). Although RALF4$_{WT}$ fully restored the fertility and pollen tube growth of the *amiralf4/19* line, RALF4$_{R89E.R90E.R91E}$ and RALF4$_{neutral\ surface}$ conferred a moderate or severe reduction in vivo, respectively (Fig. 3, E to H) but nevertheless maintained their capacity to direct their growth toward the ovules (*31*). The growth defect of *amiralf4/19* pollen tubes reflected a higher (not lower) growth velocity and premature bursting rate. Both parameters were only partially complemented in the lines expressing RALF4$_{R89E.R90E.R91E}$ or RALF4$_{neutral\ surface}$ (fig. S13). In addition, in these lines, a large proportion of the surviving pollen tubes did not show continuous oscillatory growth (*32*) but rather a stop-and-go growth pattern often followed by bursting (Fig. 3, I and J). Similar growth phenotypes were observed in the pollen LRX mutants (*33*) and in a mutant (*ppme1*) with impaired pectin demethylesterification

(*5*, *34*) (fig. S14). These data suggest that the interaction of LRX-RALF4 with demethylesterified pectin is critical for pollen tube cell wall integrity and growth.

To investigate the impact of impaired pectin interaction on cell wall patterning, we studied the cell walls of surviving pollen tubes in *amiralf4/19*–complemented lines with $RALF4_{neutral\ surface}$. Immunolabeling experiments showed a wild-type spatial localization of pectin epitopes in *amiralf4/19 pRALF4::RALF4*$_{neutral\ surface}$ lines, with high-DM pectins (LM20 antibody) and no-DM pectins (LM19 antibody) at the pollen tube tip and shank, respectively (fig. S15) (*3*, *25*). dSTORM microscopy on *amiralf4/19 pRALF4:RALF4*$_{neutral\ surface}$ cell walls, labeled for low DM pectins (LM19), showed a denser array of punctae (Fig. 3, K and L) relative to the wild type, which lacked filamentous features (Fig. 2, G and H, and fig. S8). Transmission electron microscopy (TEM) on transverse sections through the shank of pollen tubes of both wild-type and *amiralf4/19* $RALF4_{WT}$ complementation lines revealed a compact cell wall with a thin inner secondary cell wall layer labeled with anti-callose antibodies. A thicker, unstructured pectic cell wall filled with patches of callose was observed in *amiralf4/19* pollen tubes (Fig. 4A and fig. S16). The expression of $RALF4_{neutral\ surface}$ did not restore a wild-type cell wall architecture, whereas $RALF4_{R89E.R90E.R91E}$ partially complemented the aberrant discontinuous structural pattern but maintained the thick callose layer and a fibrous, more loosely packed outer cell wall (Fig. 4A and fig. S16). Altogether, these results show that RALF4 is not only a signaling peptide but also a structural cell wall component that promotes the patterning of cell wall polysaccharides into a strong polymer assembly as part of the LRX8-RALF4-pectin complex.

Discussion

In this study, we have shown that cell wall polysaccharides are shaped into a reticulated network through a peptide-activated LRX8 complex that binds and condenses pectins, thus becoming an integral part of the cell wall and conferring integrity to the expandable cell wall during pollen tube growth (Fig. 4B and fig. S17). The pectin homogalacturonan, despite the considerable differences between the mechanical landscapes of plant cell walls and the animal extracellular matrix, can be considered the equivalent of animal glycosaminoglycans (GAGs). GAGs are also unbranched, charged polysaccharides that undergo compaction and rigidification through their interaction with GAG-binding cross-linking proteins (*35*, *36*). LRX8-RALF4 is a polysaccharide-binding protein complex that promotes mesoscale cell wall patterning. The particularity of this complex, as opposed to known GAG-binding proteins, lies in its modularity, with a polycationic peptide activating the LRX8 cell wall protein to bind polyanionic pectic polysaccharides. The LRX8-RALF4-pectin interaction appears to be essential for cell wall patterning and pollen tube growth in plants, as shown by the failure of the $RALF4_{R89E.R90E.R91E}$ and $RALF4_{neutral\ surface}$ variants to restore normal cell wall organization, growth, and fertility to *amiralf4/19* pollen tubes, where the severity of the complemented phenotype scales with the severity of the homogalacturonan-binding defect.

The RALF4 peptide is molded through its interaction with LRX8, thus exposing at the surface of the heterotetramer two patches of cationic residues with an affinity for polyanionic homogalacturonan. The charge-dependent compaction of the pectin matrix may combine polyelectrolyte complex formation (also observed for the unstructured free peptide) and homogalacturonan cross-linking by the LRX8-RALF4 heterotetramer. The latter is suggested by the reduced binding capacity of the pectin layer for monomerized LRX8-RALF4 (shown by QCM-D) relative to the native complex despite a comparable affinity for isolated OGs, as shown by calorimetry and TSAs. This property might be critical for LRX8-RALF4 bioactivity given the unability of the LRX8 monomer to complement the fertility phenotype of the *lrx* quadruple mutant (*10*).

Pollen tube growth involves a balancing act among cell wall assembly, consolidation, and turgor-driven wall expansion (*2*, *3*). We propose that the web-like LRX-RALF-pectin network constitutes a load-bearing component of the pollen tube cell wall, perhaps compensating for its low cellulose content (*3*, *37*). Disruption of this network causes the pollen tube to burst, in particular during the transition from the style into the transmitting tract (*18*). In this context, it is notable that LRX proteins comprise, in addition to a RALF-binding leucine-rich repeat domain, an extensin domain (*10*, *33*, *38*). Extensins are hydroxyproline-rich, periodically amphiphilic proteins, often with YXY motifs that can form extensin peroxidase-catalyzed, di-isodityrosine intermolecular cross-links with other extensins (*39*–*42*). At least one extensin (AtEXT3) has been shown to form a dendritic scaffold in vitro. Because of the polybasic nature of AtEXT3, it was hypothesized that this scaffold may structure the cell wall by creating pectin-extensin coacervates, which may be consolidated by oxidative cross-linking between extensins (*43*). The extensin domain of LRX8 contains cross-linking acceptor tyrosine residues, but it is much less charged than AtEXT3 (17 His residues versus 91 His or Lys residues in AtEXT3). We propose that LRX8 co-opts the positive charges of the polybasic RALF4 peptide to mediate specific pectin interactions. This modularity has two obvious advantages. First, it creates the possibility of targeting the LRX-extensin network to different cell wall polymers or polymer motifs by exchanging the RALF peptide. A large number of RALF peptides have the capacity to bind to the conserved binding pocket of LRX proteins, exposing distinct surface patches (*10*). This could contribute to the patterning of cell-type–specific cell walls or cell wall domains with different architectures, such as the reticulated homogalacturonan network shown in onion cell walls or the pectin nanofilaments in epidermal cells (*27*, *44*). The second advantage is that the modularity would allow rapid regulation of cell wall assembly by monitoring free RALF peptides, which may feed back to cellular processes that control actin dynamics, as well as secretion and modification of cell wall polymers, through the low-affinity LLG/BUPS/ANX receptor complexes (*12*, *16*, *45*–*52*). Future studies could investigate under which conditions free RALF peptides are released or transferred to instruct the *Cr*RLK1Ls and LRX complexes and how this informs the cell on the status of the cell wall assembly process during cell expansion and morphogenesis. In one possible scenario, pectin could connect LLG/*Cr*RLK1L to LRX-RALF complexes, thus forming a mechanosensing cell wall network (*45*). Supporting this scenario, a direct interaction between pectin and *Cr*RLK1Ls has been reported (*53*). This interaction is most likely weak, at least for the *Cr*RLK1Ls ANX1 and BUPS1, because it escaped detection by calorimetry or TSAs (*20*, *21*) when tested with different OGs or polygalacturonic acid (fig. S18) (*54*). Nevertheless, such a weak interaction might be suitable for supporting a role in mechanosensing, for example, by detecting the deformation of the LRX-RALF-pectin network. This study uncovers the unique dual signaling and structural role of RALF4 in shaping cell wall assembly during cell expansion and morphogenesis and may provide inspiration to uncover additional roles for protein-polysaccharide interactions in defining cell wall architecture and properties.

REFERENCES AND NOTES

1. M. A. Atmodjo, Z. Hao, D. Mohnen, *Annu. Rev. Plant Biol.* **64**, 747–779 (2013).
2. P. Fayant *et al.*, *Plant Cell* **22**, 2579–2593 (2010).
3. Y. Chebli, M. Kaneda, R. Zerzour, A. Geitmann, *Plant Physiol.* **160**, 1940–1955 (2012).
4. E. Parre, A. Geitmann, *Planta* **220**, 582–592 (2005).
5. N. Röckel, S. Wolf, B. Kost, T. Rausch, S. Greiner, *Plant J.* **53**, 133–143 (2008).
6. G. Pearce, D. S. Moura, J. Stratmann, C. A. Ryan Jr., *Proc. Natl. Acad. Sci. U.S.A.* **98**, 12843–12847 (2001).
7. M. Haruta, G. Sabat, K. Stecker, B. B. Minkoff, M. R. Sussman, *Science* **343**, 408–411 (2014).
8. E. Murphy *et al.*, *J. Exp. Bot.* **67**, 4863–4875 (2016).
9. M. A. Mecchia *et al.*, *Science* **358**, 1600–1603 (2017).
10. S. Moussu *et al.*, *Proc. Natl. Acad. Sci. U.S.A.* **117**, 7494–7503 (2020).
11. M. Gonneau *et al.*, *Curr. Biol.* **28**, 2452–2458.e4 (2018).
12. Z. Ge *et al.*, *Science* **358**, 1596–1600 (2017).
13. S. Schoenaers *et al.*, *Curr. Biol.* **28**, 722–732.e6 (2018).
14. M. Stegmann *et al.*, *Science* **355**, 287–289 (2017).
15. A. Herger *et al.*, *PLOS Genet.* **16**, e1008847 (2020).
16. Z. Ge *et al.*, *Curr. Biol.* **29**, 3256–3265.e5 (2019).

17. B. C. W. Crawford, G. Ditta, M. F. Yanofsky, *Curr. Biol.* **17**, 1101–1108 (2007).
18. I. Fobis-Loisy, Y. Jaillais, *Dev. Cell* **56**, 873–875 (2021).
19. A. Geitmann, *Sex. Plant Reprod.* **23**, 63–71 (2010).
20. C. J. Layton, H. W. Hellinga, *Protein Sci.* **20**, 1439–1450 (2011).
21. P. J. Sandoval, J. Santiago, *Plant Physiol.* **182**, 1697–1712 (2020).
22. M. Bosch, A. Y. Cheung, P. K. Hepler, *Plant Physiol.* **138**, 1334–1346 (2005).
23. E. Betzig *et al*., *Science* **313**, 1642–1645 (2006).
24. M. J. Rust, M. Bates, X. Zhuang, *Nat. Methods* **3**, 793–796 (2006).
25. Y. Verhertbruggen, S. E. Marcus, A. Haeger, J. J. Ordaz-Ortiz, J. P. Knox, *Carbohydr. Res.* **344**, 1858–1862 (2009).
26. K. Palacio-Lopez *et al*., *Front. Plant Sci.* **11**, 1032 (2020).
27. K. T. Haas, R. Wightman, E. M. Meyerowitz, A. Peaucelle, *Science* **367**, 1003–1007 (2020).
28. F. Dardelle *et al*., *Plant Physiol.* **153**, 1563–1576 (2010).
29. Y.-Q. Li *et al*., *Planta* **200**, 41–49 (1996).
30. M. C. Dixon, *J. Biomol. Tech.* **19**, 151–158 (2008).
31. S. Okuda *et al*., *Nature* **458**, 357–361 (2009).
32. J. A. Feijó *et al*., *BioEssays* **23**, 86–94 (2001).
33. T. N. Fabrice *et al*., *Plant Physiol.* **176**, 1981–1992 (2018).
34. G.-W. Tian, M.-H. Chen, A. Zaltsman, V. Citovsky, *Dev. Biol.* **294**, 83–91 (2006).
35. R. P. Richter, N. S. Baranova, A. J. Day, J. C. Kwok, *Curr. Opin. Struct. Biol.* **50**, 65–74 (2018).
36. J. J. Walkowiak, M. Ballauff, R. Zimmermann, U. Freudenberg, C. Werner, *Biomacromolecules* **21**, 4615–4625 (2020).
37. H. Schlupmann, A. Bacic, S. M. Read, *Plant Physiol.* **105**, 659–670 (1994).
38. C. Ringli, *Plant J.* **63**, 662–669 (2010).
39. J. D. Brady, I. H. Sadler, S. C. Fry, *Biochem. J.* **315**, 323–327 (1996).
40. M. A. Held *et al*., *J. Biol. Chem.* **279**, 55474–55482 (2004).
41. S. Moussu, G. Ingram, *Cell Surf.* **9**, 100094 (2023).
42. D. T. A. Lamport, M. J. Kieliszewski, Y. Chen, M. C. Cannon, *Plant Physiol.* **156**, 11–19 (2011).
43. M. C. Cannon *et al*., *Proc. Natl. Acad. Sci. U.S.A.* **105**, 2226–2231 (2008).
44. W. J. Nicolas *et al*., *Curr. Biol.* **32**, 2375–2389.e6 (2022).
45. X. Zhou *et al*., *Dev. Cell* **56**, 1030–1042.e6 (2021).
46. N. Luo *et al*., *Nat. Commun.* **8**, 1687 (2017).
47. A. Boisson-Dernier *et al*., *PLOS Biol.* **11**, e1001719 (2013).
48. L. Zhu *et al*., *Plant J.* **95**, 474–486 (2018).
49. Y. J. Lee, A. Szumlanski, E. Nielsen, Z. Yang, *J. Cell Biol.* **181**, 1155–1168 (2008).
50. S. T. McKenna *et al*., *Plant Cell* **21**, 3026–3040 (2009).
51. Y. Gu *et al*., *J. Cell Biol.* **169**, 127–138 (2005).
52. Y. Gu, V. Vernoud, Y. Fu, Z. Yang, *J. Exp. Bot.* **54**, 93–101 (2003).
53. W. Feng *et al*., *Curr. Biol.* **28**, 666–675.e5 (2018).
54. S. Moussu, S. Augustin, A.-O. Roman, C. Broyart, J. Santiago, *Acta Crystallogr. D Struct. Biol.* **74**, 671–680 (2018).

ACKNOWLEDGMENTS

We thank A. Peaucelle for insightful discussions during project development and D. Mazaud, P. le Baccon, and D. Choquet for support. dSTORM experiments were performed at the Curie Institute, Paris, and the Interdisciplinary Institute for Neurocience (IINS), Bordeaux. **Funding:** This work was supported by the University of Lausanne (J.S.); the European Research Council (WallWatchers grant 716358 to J.S. and STORMtheWALL grant 101041597 to K.T.H.); the Swiss National Science Foundation (grant 310030_204526 to J.S. and grant CR32I3_156724 to U.G.); French Bio-Imaging (grant 2411 to K.T.H.); Agence Nationale de Recherche (Homeowall grant to H.H.); Saclay Plant Sciences (grant ANR-17-EUR-0007 to H.H. and K.T.H.); Research Foundation Flanders (grants 1225120N and G013023N); the University of Antwerp (grants BOF-KP and BOF-DOCPRO4 to K.V.); and LASERLAB-EUROPE (grant 654148 to S.S.). **Author contributions:** S.M. and H.K.L. were responsible for conceptualization, methodology, investigation, visualization, and data analysis. J.S. and S.M. performed the structural analysis and designed the RALF4 mutants. S.M. generated all transgenic lines reported in the study. S.M. and H.K.L. performed the pollen tube growth assays, TSA and ITC assays, and immunostaining experiments; prepared samples for dSTORM, AiryScan, and TEM imaging; and prepared Figs. 1; 2, A and I; 3, E to J; and 4, A to D, and the associated supplementary information. K.T.H prepared Figs. 2, B to E, G, H, and J; Fig. 3, K and L; and figs. S8 and S9. K.T.H. acquired and analyzed dSTORM data and prepared the associated figures. C.B. prepared Fig. 1, E and J, and figs. S2A, S3, S4C, and S11. C.B. purified proteins, performed ITC assays, and prepared the corresponding figures. U.R. acquired and analyzed Airyscan data and prepared the associated figures (Fig. 2F and fig. S7). D.D.B. performed the TEM sectioning and immunodetection of callose and acquired the TEM data images. T.L. and E.B. prepared pectins and OGs with different DMs. G.S.-F. generated the first generation of in vivo RALF4 mutants. U.G. provided materials and supervised the initial work on the first generation of in vivo RALF4 mutants. S.S. participated in the optimization of pollen tube growth behavior. K.V. supervised the optimization of pollen tube growth behavior. E.H. provided dSTORM support. N.G. supervised the Airyscan data acquisition and analysis. B.C. provided QCM-D expertise and supported data analysis. H.H. and T.L. performed the QCM-D experiments and data analysis and prepared the associated figures. H.H. and T.L. prepared Fig. 3, A to D, and fig. S10. J.S. and H.H. were responsible for conceptualization, supervision, funding acquisition, and project administration. J.S. and H.H. wrote the original draft. All authors reviewed and edited the manuscript. **Competing interests:** The authors declare no competing interests. **Data and materials availability:** All data are available in the main text or the supplementary materials. Materials are available through the corresponding authors upon request. This research was funded in whole or in part by the European Research Council (grants 716358 and 101041597), the Swiss National Science Foundation (grant 310030_204526), Agence Nationale de Recherche (grant "Homeowall"), Saclay Plant Sciences (grant ANR-17-EUR-0007), and the Swiss National Science Foundation (grant CR32I3_156724), all cOAlition S organizations. The author will make the Author Accepted Manuscript (AAM) version available under a CC BY public copyright license.

SUPPLEMENTARY MATERIALS

science.org/doi/10.1126/science.adi4720
Materials and Methods
Figs. S1 to S18
References (*55*–*63*)
MDAR Reproducibility Checklist

Submitted 27 April 2023; accepted 22 September 2023
10.1126/science.adi4720